A CMOS Optical Preamplifier for Wireless Infrared Communications

Khoman Phang and David A. Johns, *Senior Member, IEEE*

***Abstract*— This paper describes a CMOS optical preamplifier suitable for infrared wireless data communications. The preamplifier consists of a differential CMOS variable-gain transimpedance amplifier embedded in a larger feedback loop used to reject photocurrents generated by ambient light. Fabricated in a commercial 0.35-μm CMOS process, the preamplifier consumes 8 mW at 3 V, and provides 70-MHz bandwidth over a 77-dB dynamic range with a maximum transimpedance gain of 19 kΩ. The bandwidth is controlled within a factor of two over a 31-dB variation in gain.**

***Index Terms*—Ambient photocurrent rejection, CMOS-optical preamplifier, infrared wireless communications, variable-transimpendance amplifier.**

I. Introduction

THE proliferation of free space, infrared (IR) wireless data links in laptop computers, computer peripherals, and digital cameras has helped drive new developments in optical receiver design. While traditional applications such as fiber-optic networks have emphasized speed, IR wireless communications emphasizes system integration and low cost. Consequently, commercial digital CMOS is preferred over higher speed technologies, such as GaAs or bipolar.

The three principal requirements of an IR wireless preamplifier are a wide bandwidth, a wide dynamic range, and the ability to reject ambient light. IR wireless receivers have more modest bandwidth requirements than fiber-optic receivers. This is due to the need to keep costs low and the fact that relatively large photodiodes are required in order to make up for the path losses that occur over free-space transmission. Current Infrared Data Association (IrDA) standards support data rates of 4 Mb/s [1], and future standards for rates of 100 Mb/s and higher are being investigated. A wide dynamic range is essential in order to accommodate variable link distances. IrDA standards allow a range of 0–100 cm, over which the signal power may vary by five orders of magnitude [1]. Since the receiver is meant to operate in the user environment, it must be able to detect signals even in the presence of strong ambient light. In situations where the signal is weak, the photocurrent generated by ambient light can overwhelm the signal. IrDA standards specify a maximum ambient light level that is more than 100 times larger than the minimum signal.

Manuscript received October 18, 1998; revised March 9, 1999. This work was supported in part by Micronet and the Natural Sciences and Engineering Research Council of Canada. This paper was recommended by Guest Editors F. Maloberti and A. Baschirotto.

The authors are with the Department of Electrical and Computer Engineering, University of Toronto, Toronto, ON, M5S 3G4 Canada.

Publisher Item Identifier S 1057-7130(99)05647-5.

A wide bandwidth and dynamic range can be achieved in part by using a transimpedance amplifier as the preamplifier stage of the receiver [2]. However, the inherent dynamic range of a fixed-transimpedance amplifier is typically not sufficient for an IR wireless receiver. Techniques that extend the dynamic range right at the preamplifier include varying the preamplifier gain [3], [4], and placing a variable signal attenuator before the preamplifier [5], [6]. The second technique uses a bipolar differential pair as a current attenuator. Bipolar transistors are required because their exponential voltage-to-current characteristic ensures a well-regulated photodiode bias voltage across many orders of magnitude. The need for bipolar transistors makes this technique unsuitable for CMOS. The first technique, however, poses its own set of challenges. Reported variable-gain transimpedance amplifiers based on traditional designs are difficult to stabilize [3], [4]. As a result, they require multiple variable resistors that are heuristically fine tuned, making these circuits difficult to design and prone to modeling errors. This paper presents a two-stage, differential transimpedance amplifier whose stability depends only on the tracking of identical pairs of resistors. In contrast to the designs reported in [3] and [4], the bandwidth of this amplifier is well controlled over the entire gain range. Controlling the bandwidth improves sensitivity by rejecting out-of-band noise without the need for additional filtering. Although a constant-bandwidth variable-gain transimpedance amplifier was presented in [7], experimental results for that work have yet to be reported.

There are two main alternatives for rejecting ambient light at the preamplifier. One solution is to place a high-pass resistance–capacitance (*RC*) network at the input of the preamplifier, as shown in Fig. 1(a) [6], [8], [9]. Here, the high-frequency signal current i_s passes through while the dc component $I_{\rm dc}$ is blocked and shunted away through resistor R. This solution has two major drawbacks. First, for monolithic implementations, large on-chip resistors and capacitors are required to achieve sufficiently low cutoff frequencies. These passive elements occupy area and are sensitive to parasitic-coupled noise. Second, the bias voltage across the photodiode varies with the average photocurrent since the voltage at the anode is given by $I_{\rm dc} \times R$. As a result, the overall receiver bandwidth is affected by the signal and ambient light levels.

The alternative to a passive *RC* network is to use an active feedback loop around the transimpedance amplifier, as shown in Fig. 1(b). Level detection based on the peaks of the signal is effective [10], [11], but assumes that the average current is constant and requires a reset mechanism.

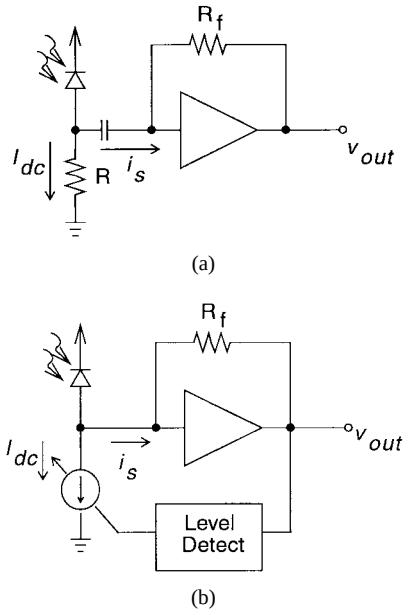

Fig. 1. Ambient photocurrent rejection techniques. (a) Passive *RC* network. (b) Active feedback loop.

An alternative is to use average-level detection. Although this is essentially achieved in the preamplifier presented in [12], the resulting dc rejection is more of a side effect of the biasing requirement of the preamplifier. This paper presents an alternative structure in which the feedback loop does not impose constraints on the design of the transimpedance amplifier. The resulting ambient light-rejection circuit requires less area, and effectively regulates the photodiode bias voltage.

In the next section, we describe the basic architecture of the preamplifier and analyze the ambient photocurrent rejection circuit. The differential variable-gain transimpedance amplifier is discussed in Section III. Section IV provides details of the fabricated test chip and presents the experimental results.

II. Ambient Photocurrent Rejection Circuit

The optical preamplifier with ambient photocurrent rejection is shown in Fig. 2. The transimpedance amplifier converts the current from the photodiode into a differential voltage. Surrounding the amplifier is an outer feedback loop comprised of an error amplifier and transistor $M_{\rm ctl}$. The rejection circuit operates as follows: the dc component of the photocurrent produces an offset in the average levels of the differential outputs, as illustrated in Fig. 3(a). This offset is integrated over time by the error amplifier. Transistor $M_{\rm ctl}$ acts as a variable-current sink which, at steady-state, eliminates the average photocurrent, $I_{\rm dc}$ from the signal path, as shown in Fig. 3(b). The average photocurrent consists of the ambient photocurrent and the dc component of the signal.

Using a differential signal path helps maximize the preamplifier's immunity to noise from the power supply and substrate. The photodiode, however, is connected to only one terminal. This creates an asymmetry at the input of the differential structure. As a result, an additional capacitor C_d' is required at the other input of the transimpedance amplifier in order to match the photodiode capacitance and to rebalance

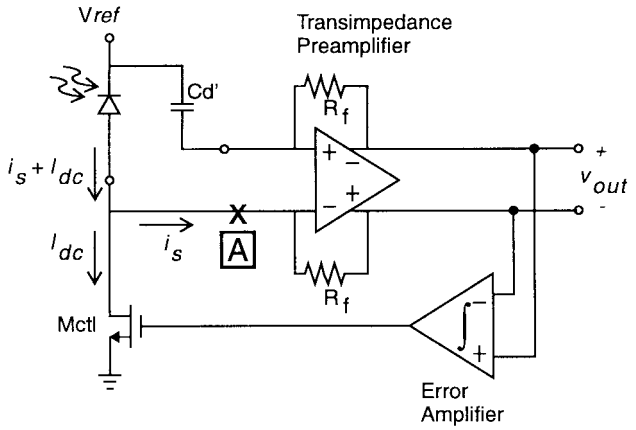

Fig. 2. Optical preamplifier with ambient photocurrent rejection.

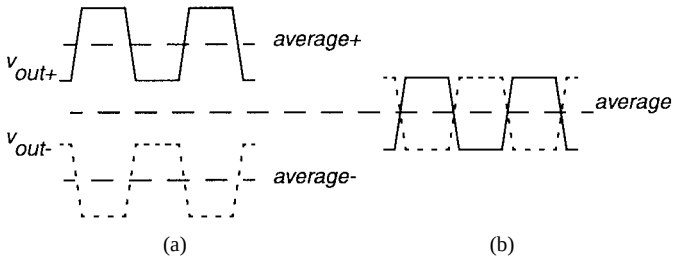

Fig. 3. Differential output waveforms. (a) Without ambient photocurrent rejection. (b) With rejection.

the circuit. Perfect matching ensures that noise injected at the bias voltage $V_{\rm ref}$ appears as a common-mode signal that is effectively rejected by the differential structure. In practice, however, some mismatch can be expected, and additional measures such as adding an on-chip tuning capacitor [13] may be required to improve matching.

The characteristics of the ambient photocurrent rejection circuit can be studied by breaking the loop at point A in Fig. 2. At low-to-midband frequencies where the feedback loop is effective, the loop gain is given by

$$L(s) = A_{\rm timp} \times A_{\rm err}(s) \times g_{\rm mctl} \tag{1}$$

where $A_{\rm timp}$ is the passband gain of the transimpedance amplifier, and $g_{\rm mctl}$ is the transconductance of $M_{\rm ctl}$. The gain of the error amplifier $A_{\rm err}(s)$ has a dominant-pole response

$$A_{\rm err}(s) = \frac{A_{\rm dc}}{1 + s/\omega_{p1}} \tag{2}$$

where $A_{\rm dc}$ is the dc voltage gain, and ω_{p1} is the dominant pole frequency. The resulting closed-loop response of the preamplifier with ambient rejection is

$$\frac{v_{\rm out}}{i_s}(s) = \frac{A_{\rm timp}}{1 + L(s)} \approx A_{\rm timp} \times \frac{s + \omega_{p1}}{s + A_{\rm timp}\, A_{\rm dc}\, \omega_{p1}\, g_{\rm mctl}} \tag{3}$$

where the zero at $\omega = \omega_{p1}$ is much lower than the pole at $\omega = A_{\rm timp} A_{\rm dc} \omega_{p1} g_{\rm mctl}$. Thus, the preamplifier exhibits a high-pass response with a cutoff frequency of

$$\omega_{HP} = A_{\rm timp}\, A_{\rm dc}\, \omega_{p1}\, g_{\rm mctl} \tag{4}$$

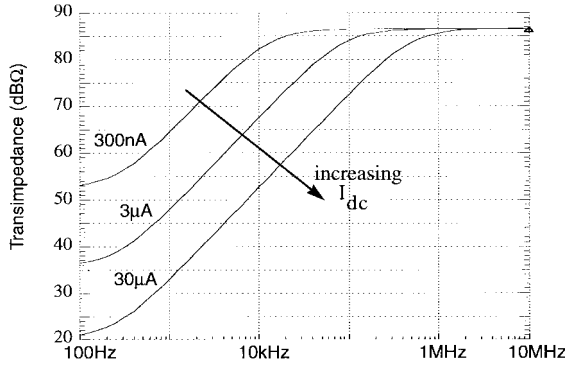

Fig. 4. Simulated frequency response of preamplifier for different average photocurrents.

a passband gain of $A_{\rm timp}$, and a dc gain of $1/A_{\rm dc}g_{\rm mctl}$. Since $M_{\rm ctl}$ is biased by current $I_{\rm dc}$, $g_{\rm mctl}$ is proportional to the square root of $I_{\rm dc}$. This leads to the interesting observation that both the preamplifier's dc gain and high-pass cutoff frequency are a function of the average photocurrent. These observations can be seen in the simulated frequency response shown in Fig. 4 for different average photocurrent levels. The simulation assumes that $A_{\rm timp} = 20$ kΩ, $A_{\rm dc} = 100$, and $\omega_{p1} = 800$ Hz. The plot clearly shows an increasing cutoff frequency and decreasing dc gain with increasing $I_{\rm dc}$.

Understanding the implications of this dependency on $I_{\rm dc}$ is easier when we consider the signal and ambient light sources separately. The most critical situation occurs when the ambient light overpowers the signal. Here, $I_{\rm dc}$ is essentially the photocurrent due to the ambient light. From Fig. 4, we can conclude that the feedback loop is self-regulating in this case, becoming more effective at rejecting ambient light as the level increases. When the level is low, the feedback loop—or more precisely, transistor $M_{\rm ctl}$—is nearly off. Since $M_{\rm ctl}$ is located right at the input, any thermal noise it generates adds directly to the signal current. Having $M_{\rm ctl}$ turn off maximizes the preamplifier's sensitivity in low ambient light. When the signal is much stronger than the ambient light, the saturation of the preamplifier can be prevented by simply adjusting the preamplifier gain. Thus, the ambient photocurrent rejection circuit is not critical here, and can be disabled or limited in order to eliminate this dependency on $I_{\rm dc}$.

An adequate phase margin is required to ensure the stability of the feedback loop. From the loop-gain expression given in (1), this is achieved by compensating the error amplifier so that ω_{p1} is low enough for maximum values of $A_{\rm timp}$ and $g_{\rm mctl}$. Besides stability, ω_{p1} must also be designed to limit the maximum high-pass cutoff frequency given in (4) in order to prevent the preamplifier from filtering the signal. An upper limit to transconductance $g_{\rm mctl}$ can be set by limiting the gate voltage—hence, current—of $M_{\rm ctl}$. This maximum current must be greater than the current generated by the photodiode under the brightest ambient light conditions (e.g., direct sunlight). Fluorescent lamps with electronic ballasts require special consideration. These lamps do not have strong emissions in the infrared spectrum, so saturation of the preamplifier is usually not a problem. However, the rapid firing of the ballasts produces interference patterns with harmonics

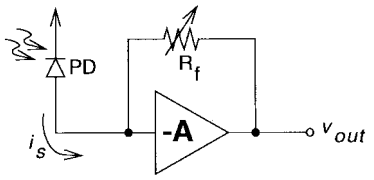

Fig. 5. Variable-gain transimpedance amplifier.

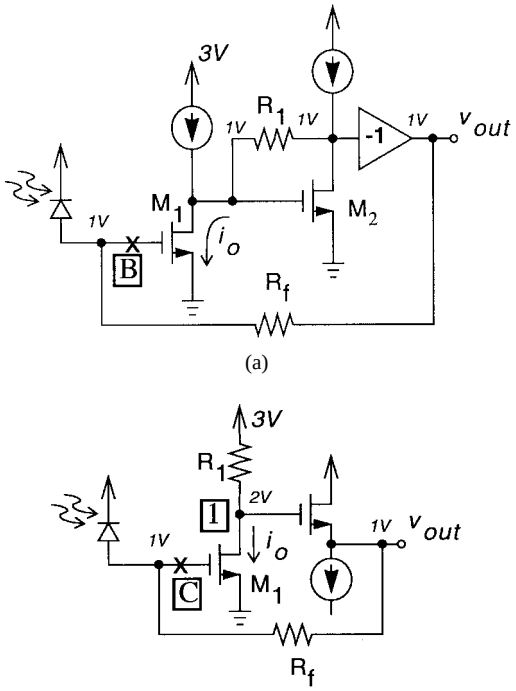

Fig. 6. Two transimpedance amplifiers. (a) Proposed (local shunt feedback). (b) Traditional.

that can reach 1 MHz [14]. Consequently, additional high-pass filtering may be needed further along in the receiver to reject this interference.

III. Differential Variable-Gain Transimpedance Amplifier

A variable-gain transimpedance amplifier is shown in Fig. 5. The passband gain is given by

$$A_{\rm timp} = \frac{v_{\rm out}}{i_s} = R_f \frac{-A}{1+A} \approx -R_f, \qquad \text{for } A \gg 1 \quad (5)$$

where A is the voltage gain of the amplifying stage. The transimpedance gain is adjusted by simply varying the feedback resistance R_f. For weak signals, R_f should be maximized to improve sensitivity, while for strong signals, R_f should be minimized to prevent saturation. The dynamic range for this amplifier could be defined as the range from the noise floor of the amplifier (using maximum R_f) to its maximum input current (at minimum R_f).

As mentioned earlier, reported variable-gain transimpedance amplifiers based on the traditional design are difficult to stabilize. Fig. 6 shows the proposed transimpedance amplifier together with the traditional two-stage design. The main difference is the shunt-feedback second stage that is used in place

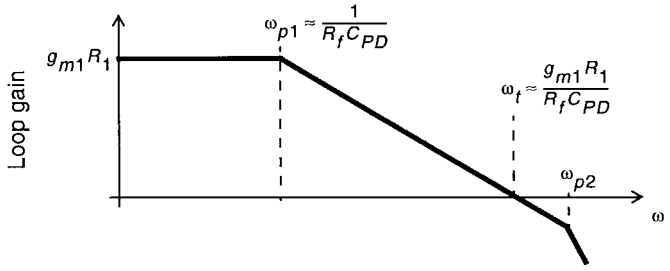

Fig. 7. Frequency plot of loop gain for both transimpedance amplifiers.

of the source follower. This structure was originally proposed by Hullett and Moustakas for fixed-gain preamplifiers [15], [16]. The three-stage design consists of a transconductance first stage, a transimpedance second stage, and an output stage that provides small-signal inversion. The overall voltage gain of the amplifier is

$$A = -\left(\frac{v_{\text{out}}}{i_o} \times \frac{i_o}{v_{\text{in}}} \times -1\right) \approx g_{m1}R_1 \tag{6}$$

which is typically in the range of ten to a few hundred. Coincidentally, the same expression is obtained for the traditional design assuming the output source follower has unity gain.

The stability of these circuits can be analyzed by breaking their feedback loops at points B and C. Fig. 7 shows the main features of the loop gain for both circuits. The frequency where the loop gain of the transimpedance amplifiers is unity is approximately

$$\omega_t \approx \frac{A}{R_f C_{\text{PD}}} \approx \frac{g_{m1}R_1}{R_f C_{\text{PD}}} \tag{7}$$

where C_{PD} is the photodiode capacitance. The stability of the amplifiers is determined by the relative position of ω_t to the nondominant pole, ω_{p2}. From (7), we see that ω_t increases when R_f is reduced. In contrast, we can assume the nondominant pole is not significantly affected by R_f. High-frequency gain peaking occurs when ω_t comes too close to ω_{p2}. To prevent this, the unity-gain frequency should track changes in R_f. Specifically, if resistor R_1 could track R_f, ω_t would remain constant and stability would be maintained. The bandwidth of the transimpedance amplifiers is approximately

$$BW \approx \frac{1+A}{R_f C_{\text{PD}}} \approx \frac{g_{m1}R_1}{R_f C_{\text{PD}}} \approx \omega_t. \tag{8}$$

Thus, having R_1 track R_f is also the condition required for maintaining a constant bandwidth. In summary, adapting either transimpedance amplifier for variable gain requires the tracking of variable resistors R_1 and R_f.

The difficulty in meeting this tracking requirement is the key difference between the two circuits. Tracking is difficult in the traditional structure for a number of reasons. First, as we can see from Fig. 6(b), the terminal voltages of R_1 and R_f are very different. Given a low supply voltage, these resistors will likely be realized with different MOSFET types to ensure that the transistors to remain in triode operation: R_1, biased close to V_{dd}, requires a p-channel, device while R_f, biased closer to ground, requires an n-channel device. Getting n- and p-channel devices to track is inherently challenging. Second, there is a voltage drop across R_1 that is not mirrored across R_f. The voltage drop occurs because R_1 is responsible for supplying the bias current of M_1. As a result, R_1 is always closer to saturation than R_f, making tracking especially difficult when the signals are large. As a result, the amplifier reported in [4] introduces a source degeneration resistor for M_1 whenever handling large signals in order to maintain stability. The voltage drop across R_1 also implies that changing R_1 changes the bias voltage on node 1. The amplifier reported in [3] attempts to solve this by leaving the original R_1 fixed, and adding another variable resistor with one terminal connected to node 1, and the other terminal connected to the equivalent node of a dummy transimpedance amplifier that is required simply in order to recreate node 1's bias voltage.

The problems involved in tracking R_1 and R_f are avoided with the proposed design because R_1 is now used as a shunt feedback resistor much in the same way as R_f. As illustrated in Fig. 6(a), the resistors have essentially identical terminal voltages, with one terminal biased at $V_{GS1,2}$ and the other terminal connected to the output. Thus both resistors can be implemented using the same type of MOSFET. Neither resistor handles any bias current, so the problem of a fixed voltage drop across R_1 is eliminated. This structure also nicely accounts for any nonlinearities in R_1 and R_f for when the MOSFET's approach saturation, they do so in conjunction and so tracking is still maintained.[1] This characteristic suggests that the structure is equally well suited for limiting amplifier designs which use nonlinear feedback elements to achieve clamping. Although R_1 and R_f can be designed to track to any fixed ratio, we can simplify the design by making R_1 and R_f equal.

Optimizing the bandwidth requires an analysis of the proposed amplifier. A small-signal model is shown in Fig. 8, where C_f is the shunt feedback capacitance across the gate and drain of M_2, and C_i and C_o are the total capacitances at the internal node and output node, respectively.

Because of the presence of the two capacitors, C_i and C_o, the second stage exhibits a second-order response. Assuming $g_{m2} \gg 1/r_{\text{ds2}}$ and $1/R_1$, and $C_f \ll C_i$ and C_o, the frequency response is approximately

$$A(s) \equiv \frac{v_{\text{out}}}{v_{\text{in}}}(s) \approx -\frac{g_{m1}}{C_i C_o} \times \frac{sC_f + (1/R_1 - g_{m2})}{s^2 + \frac{g_{m2}C_f}{C_i C_o}s + \frac{g_{m2}}{C_i C_o R_1}}. \tag{9}$$

By tuning C_f, we can make the poles of this transfer function complex, resulting in the following design equations:

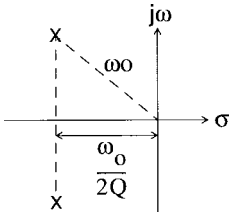

$$\omega_o \approx \sqrt{\frac{g_{m2}}{C_o C_i R_1}} \tag{10}$$

$$Q \approx \frac{1}{C_f}\sqrt{\frac{C_o C_i}{g_{m2}R_1}}. \tag{11}$$

[1] Strictly speaking, this is only true of the final differential structure, in which the inverting third stage is eliminated.

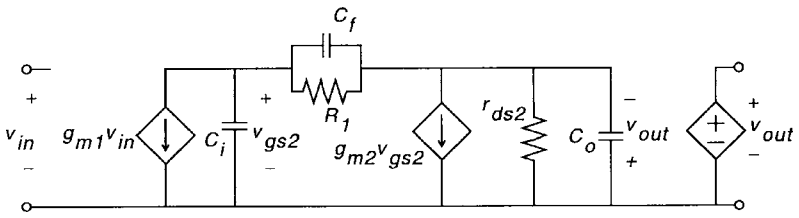

Fig. 8. Small-signal model of three-stage amplifier.

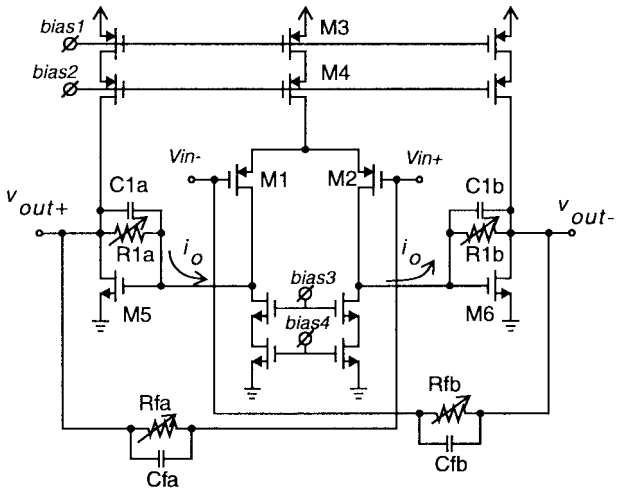

Fig. 9. Fully differential CMOS variable-transimpedance amplifier.

Typically, a variable-gain transimpedance amplifier is optimized for a desired bandwidth at its maximum gain. At lower gain settings, only the stability of the circuit needs to be confirmed. There are many ways to approach the design of this circuit. One approach would be to start with the second stage. For a given bandwidth—which, as shown earlier, is essentially equal to ω_t—we can determine the maximum value of R_1 using (10) by estimating the values of g_{m2}, C_i, and C_o, based on device geometry and power dissipation, and by choosing a nondominant pole frequency, ω_o sufficiently higher than ω_t (a reasonable choice is $\omega_o \approx 2\omega_t$). Equation (11) can then be used to find the value of C_f corresponding to the desired Q-factor (say $1/\sqrt{2} = 0.71$ for a maximally-flat response [17]). Given the photodiode capacitance $C_{\rm PD}$ and estimating g_{m1}, (7) then determines the maximum value of R_f.

The differential version of the variable-gain transimpedance amplifier is shown in Fig. 9. Compared to the single-ended version in Fig. 6(a), the transconductance first stage is now realized using a p-channel differential pair. This allows the input transistors to be placed in an isolated n-well to reduce substrate noise at the cost of slightly greater thermal noise [18]. Devices M_5 and M_6 operate single-endedly, biasing each output at around 1 V, and eliminating the need for common-mode feedback. The inverting buffer required in the single-ended design is eliminated in the differential version. Instead, small-signal inversion is accomplished by simply cross coupling the differential outputs [16]. The dynamic range, as defined earlier, is the ratio of the noise floor of the amplifier to its maximum input current. A detailed noise analysis of the single-ended circuit is provided in [15] for reference. The maximum signal current is determined by the tail current of the input differential pair. This is because the differential signal current that passes through $R_{fa,b}$ is essentially mirrored to the internal current i_o that passes through $R_{1a,b}$. Current i_o is supplied by the differential pair and so is limited to half the tail current.

IV. Experimental Results

We implemented a test chip to demonstrate a 100-Mb/s IR wireless link. The transimpedance amplifier is designed to provide a maximum gain of 20 kΩ over a 70-MHz bandwidth. We assume an input capacitance of 5 pF, which is typical of large photodiodes used in IR wireless receivers. The ambient photocurrent rejection circuit is designed to handle up to 30 μA, which corresponds to a typical 10-mm^2 Si-PIN photodiode being exposed to direct sunlight. The maximum high-pass cutoff frequency is 1 MHz, which is sufficiently low for a 100-Mb/s nonreturn to zero (NRZ) signal with some form of run length limiting to prevent the transmission of long strings of one's or zero's. Alternatively, some form of baseline wander correction can be used. In order to keep the power dissipation below 10 mW, we limit the tail current of the transimpedance amplifier's input differential pair to 800 μA. This sets the maximum input current to 400 μA. With a transimpedance gain of 500 Ω, 400 μA produces an output of 200 mV. Hence, the variable-transimpedance amplifier is designed to provide gains from 20 kΩ (86 dBΩ) down to 500 Ω (54 dB$\cdot\Omega$), a gain range of 32 dB.

The four variable resistors of the transimpedance amplifier are identical. In order to realize the desired gain range, each resistor is comprised of three pairs of pass transistors, as illustrated in Fig. 10(a). Each pass transistor can either be turned off or set to one of two resistance values by controlling the gate bias voltages as shown in Fig. 10(b). With three differently scaled pass transistors, each having three settings, the digitally-controlled pass-transistor array has the ability to realize $3^3 = 27$ different resistance values. In order to maximize linearity, complementary n- and p-channel MOSFET's are used, and the n-wells of the p-channel devices are tied to the output of the array to eliminate the body effect. A penalty in speed of about 40% is incurred as a result of the added capacitance due to the n-wells. Simulations show that the variable resistor remains within $\pm$10% of its nominal value for voltage drops within $\pm$0.3 V. Device $M_{\rm tap}$ acts as a series resistor. By driving the error amplifier from the middle tap terminal of resistors $R_{\rm fa}$ and $R_{\rm fb}$ instead of from their outputs, we effectively reduce the loop gain of the ambient photocurrent rejection circuit, thereby lowering the high-pass

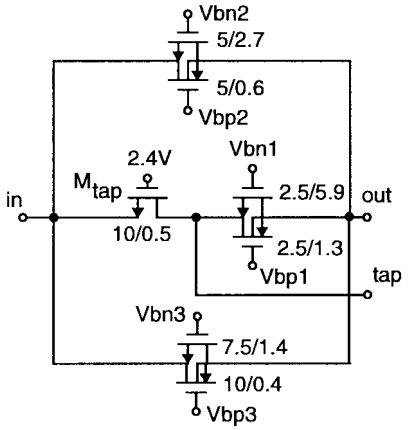

(a)

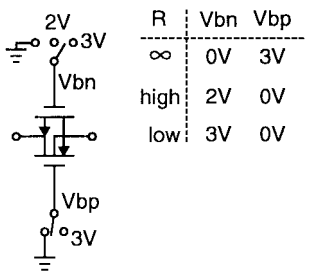

(b)

Fig. 10. (a) Pass-transistor array used to implement variable resistor. (b) Detail of pass transistor. *W/L* dimensions are given in units of micrometers.

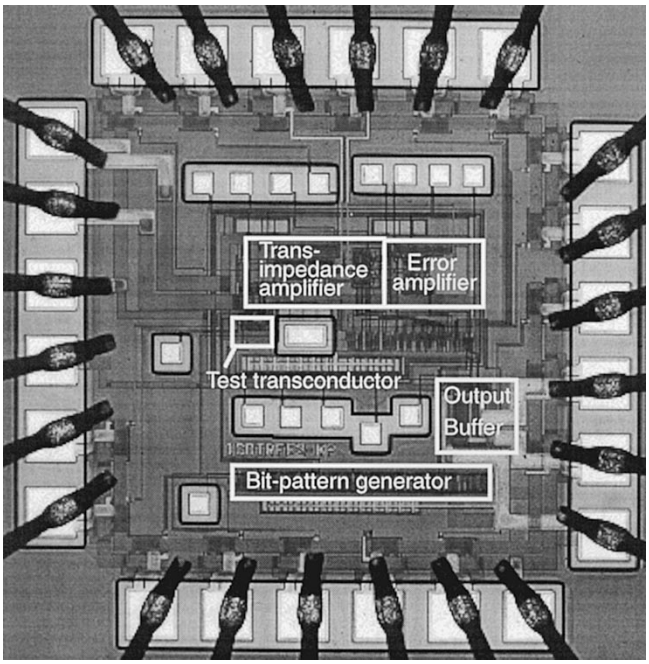

Fig. 11. Micrograph of test chip.

cutoff frequency. Simulations show that a series resistance of 500 Ω or less is required to keep the cutoff frequency below 1 MHz in the presence of a 30-μA average photocurrent.

The preamplifier was fabricated in a commercial 0.35-μm digital CMOS process. The test chip which occupies 1.44 mm^2 is shown in Fig. 11. The chip includes a bit-pattern generator, test transconductor, and an open-drain, differential output buffer that also serves as an LED driver. The error amplifier is a common two-stage CMOS opamp with a 5-pF internal compensation capacitor [18]. Simulations show it has a dc gain of 94 dB and a dominant pole at 150 Hz.

TABLE I
MEASURED PERFORMANCE OF PREAMPLIFIER

Technology	0.35 μm digital CMOS
Supply voltage	3 V
Bandwidth	70 MHz ±20 %
Transimpedance	19kΩ–500Ω
Input noise current density	6.7 $pA/\sqrt{Hz}$
Input capacitance	5 pF
Maximum signal current	400 μA
Preamplifier active area	0.04 mm^2
Power dissipation	8 mW (preamplifier)
	43 mW (output buffer)

Fig. 12 plots the measured frequency response of the variable-gain transimpedance amplifier together with typical simulation results. A sensitivity study in SPICE using fast and slow MOSFET models, together with a temperature range from 0 °C to 80 °C, showed a ±10% bandwidth and ±25% gain deviation from the typical performance. The measured results are consistent with the simulations within the passband. With a maximum gain of 19 kΩ, the preamplifier has a measured gain range of 31 dB. Simulations results predict that over the gain range the bandwidth varies from 68 to 130 MHz while measured results show a tighter span from 85 to 103 MHz. In either case, the bandwidth is still controlled to within a factor of two. At any gain setting, the transimpedance amplifier's response is well behaved, showing no significant peaking. A total input-referred noise current of 56 nA was measured at the maximum gain. This translates to an average input-noise current density of 6.7 pA/$\sqrt{\text{Hz}}$, which is reasonably close to our simulated result of 5.3 pA/$\sqrt{\text{Hz}}$. With a 56-nA noise floor and a maximum input-current handling of 400 μA, the preamplifier has a dynamic range of 77 dB (38 dB optical).

Fig. 13 shows the eye diagram for a 100-Mb/s optical link constructed from two test chips (one for transmit and the other for receive), a Mitel 1A301 infrared LED, and a Mitel 1A354 Si-PIN photodiode.[2] The performance of the ambient photocurrent rejection loop is illustrated in the step response shown in Fig. 14. Here, a 10-μA dc current is injected into the preamplifier. The ambient photocurrent rejection circuit is initially disabled, and then activated at the indicated point on the graph. The total settling time is 6 μs, which agrees with simulation. Table I summarizes the measured performance of the circuit.

Table II places this work alongside other recent fixed and variable-gain transimpedance amplifiers. To our knowledge, variable-gain transimpedance amplifiers reported to date have all been single-ended designs fabricated in either bipolar or BiCMOS technology, and have not been designed for supply voltages lower than 5 V. The differential CMOS transimpedance amplifier presented by Tanabe *et al.* [10] could be adapted to have variable gain. With only one gain

[2] The 1A354 has a typical capacitance of only 1 pF so additional capacitance was added to increase the input capacitance to 5 pF. The original photodiode that we had designed for has a lower bandwidth than the data sheet would indicate.

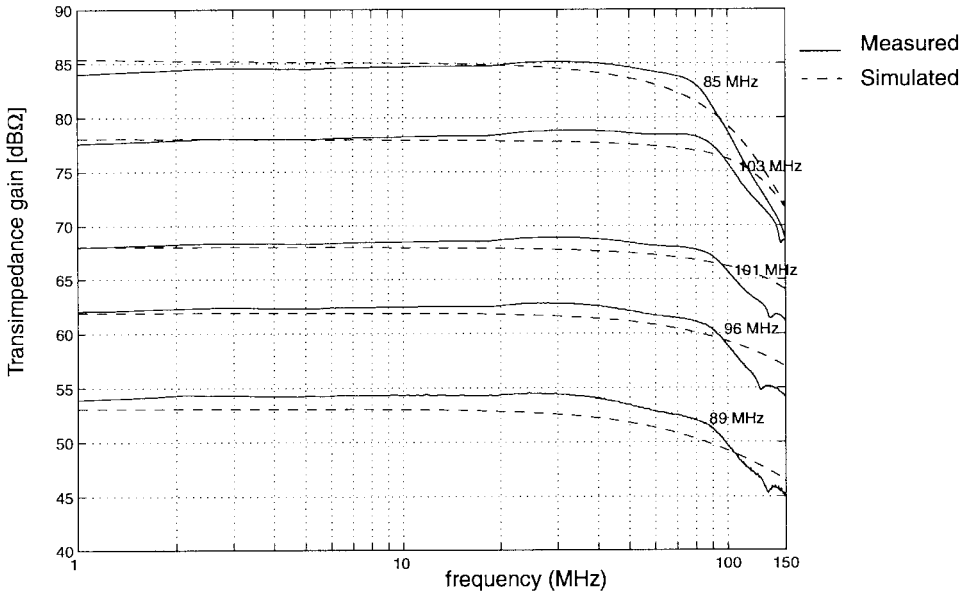

Fig. 12. Simulated and measured frequency response of transimpedance amplifier.

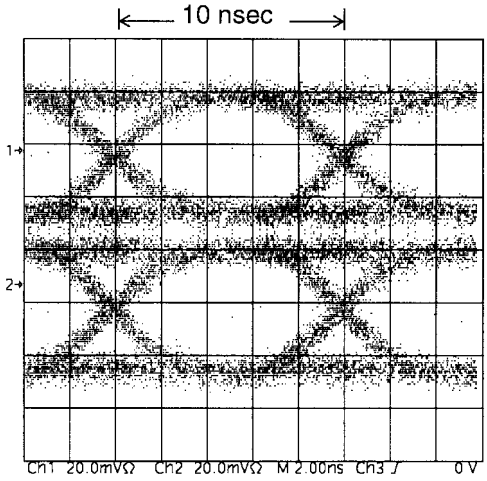

Fig. 13. Eye diagram for 100-Mb/s optical link with 19-kΩ transimpedance gain.

stage, the circuit's stability is ensured, albeit possibly at the cost of reduced bandwidth. The transimpedance amplifier presented by Ingels *et al.* [19] has varying gain, but the gain variations are uncontrolled, making the circuit more of a limiting amplifier rather than a true variable-gain design. The proposed circuit has the lowest power dissipation. Despite the large input capacitance, it achieves a bandwidth of 70 MHz that is sufficient for a 100-Mb/s data rate. Finally, it is the only implemented variable-gain design with a well regulated bandwidth.

V. Summary

An optical preamplifier suitable for IR wireless data communications has been presented. We have proposed an alternative structure for variable-gain transimpedance amplifiers. This structure exhibits improved control of stability and bandwidth. We have also described a method of rejecting ambient light by using active feedback around the transimpedance amplifier.

TABLE II
A Comparison of Various Recent Transimpedance Amplifiers

Reference	Outputs	Process	Power (mW)	Supply (V)	DR (dB)	Cin (pF)	Gain (kΩ)	Bandwidth (MHz)
[3]	single	BiCMOS	110	5	107	1.0	98 ~ 0.16	128
[4]	single	BiCMOS	>120	5	>80	0.4	10.7 ~ 0.4	600
[10]	differential	CMOS	22	2	--	0.3	1.6 ~ 0.4	1900
[5]	single	Bipolar	--	--	73	2.0	1	220
[6]	single	BiCMOS	<250	5	80	6.7	260 ~ 1.1	170
[19]	single	CMOS	20	5	--	1.0	150	120
This work	**differential**	**CMOS**	**8**	**3**	**77**	**5.0**	**19 ~ 0.5**	**70**

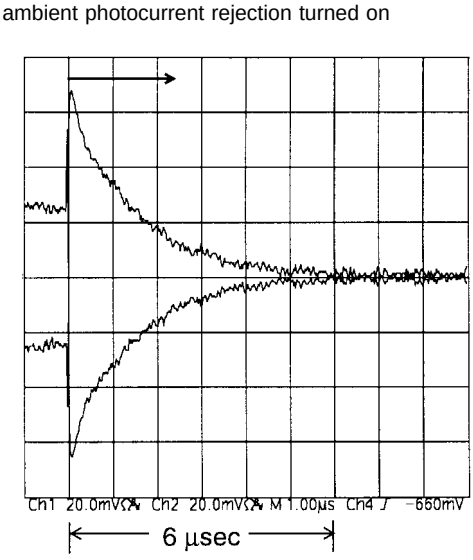

Fig. 14. Measured step response of the ambient photocurrent-rejection circuit to 10-μA dc input.

Experimental results from a test chip fabricated in 0.35-μm CMOS were presented. The preamplifier consumes 8 mW at 3 V, and provides 70-MHz bandwidth over a 77-dB dynamic range with a maximum transimpedance gain of 19 kΩ. The bandwidth is controlled to within a factor of two over a 31-dB variation in gain.

ACKNOWLEDGMENT

The authors would like to thank to D. Mundae of Mitel Corporation for providing them with the optoelectronic components used in the experimental optical link. The authors also thank the Canadian Microelectronics Corporation (CMC) for helping to fabricate the design.

REFERENCES

[1] Infrared Data Association. (1997). *Serial Infrared Physical Layer Link Specification*, Version 1.2. [Online.] Available HTTP: http://www.irda.org

[2] J. L. Hullett and T. V. Muoi, "A feedback receive amplifier for optical transmission systems," *IEEE Trans. Commun.*, vol. COM-24, pp. 1180–1185, Oct. 1976.

[3] R. G. Meyer and W. D. Mack, "A wideband low-noise variable-gain BiCMOS transimpedance amplifier," *IEEE J. Solid-State Circuits*, vol. 29, pp. 701–706, June 1994.

[4] H. Khorramabadi, L. D. Tzeng, and M. J. Tarsia, "A 1.06 Gb/s-31 dBm to 0dBm BiCMOS optical preamplifier featuring adaptive transimpedance," *IEEE ISSCC Dig. Tech. Papers*, pp. 54–55, Feb. 1995.

[5] L. A. D. van den Broeke and A. J. Nieuwkerk, "Wide-band integrated optical receiver with improved dynamic range using a current switch at the input," *IEEE J. Solid-State Circuits*, vol. 28, pp. 862–864, July 1993.

[6] P. Palojarvi, T. Ruotsalainen, and J. Kostamovaara, "A variable gain transimpedance amplifier channel with a timing discriminator for a time-of-flight laser radar," in *Proc. Euro. Solid-State Circuits Conf.*, Southampton, U.K., Sept. 1997, pp. 384–387.

[7] B. Wilson and J. D. Drew, "Novel transimpedance amplifier formulation exhibiting gain-bandwidth independence," in *IEEE Proc. Int. Symp. Circuits Systems*, June 1997, vol. 1, pp. 169–172.

[8] M. B. Ritter, F. Gfeller, W. Hirt, D. Rogers, and S. Gowda, "Circuit and system challenges in IR wireless communication," in *IEEE ISSCC Dig. Tech. Papers*, pp. 398–399, Feb. 1996.

[9] C. Petri, S. Rocchi, and V. Vignoli, "High dynamic CMOS preamplifiers for QW diodes," *Electron. Lett.*, vol. 34, no. 9, pp. 877–878, Apr. 1998.

[10] A. Tanabe, M. Soda, Y. Nakahara, A. Furukawa, T. Tamura, and K. Yoshida, "A single chip 2.4 Gb/s CMOS optical receiver IC with low substrate crosstalk preamplifier," in *IEEE ISSCC Dig. Tech. Papers*, pp. 304–305, Feb. 1998.

[11] R. G. Swartz, Y. Ota, M. J. Tarsia, and V. D. Archer, "A burst mode, packet receiver with precision reset and automatic dark level compensation for optical bus communications," in *Proc. Symp. VLSI Technology*, Kyoto, Japan, May 1993, pp. 67–68.

[12] E. Brass, U. Hilleringmann, and K. Schumacher, "System integration of optical devices and analog CMOS amplifiers," *IEEE J. Solid-State Circuits*, vol. 29, pp. 1006–1010, Aug. 1994.

[13] T. Yoon and B. Jalali, "1.25 Gb/s CMOS differential transimpedance amplifier for gigabit networks," in *Proc. Eur. Solid-State Circuits Conf.*, Southampton, U.K., Sept. 1997, pp. 140–143.

[14] A. J. C. Moreira, R. T. Valadas, and A. M. de Oliveira Duarte, "Optical interference produced by artificial light," *Wireless Networks*, vol. 3, pp. 131–140, 1997.

[15] J. L. Hullett and S. Moustakas, "Optimum transimpedance broadband optical preamplifier design," *Opt. Quantum Electron.*, vol. 13, pp. 65–69, 1981.

[16] R. Coppoolse, J. Verbeke, P. Lambrecht, J. Codenie, and J. Vandewege, "Comparison of a bipolar and a CMOS front end in broadband optical transimpedance amplifiers," in *Proc. 38th Midwest Symp. Circuits and Systems*, Brazil, Aug. 1996, pp. 1026–1029.

[17] A. S. Sedra and K. C. Smith, *Microelectronic Circuits*, 4th ed. Oxford, U.K.: Oxford Univ. Press, 1997, pp. 718–722.

[18] D. A. Johns and K. W. Martin, *Analog Integrated Circuit Design.* New York: Wiley, 1997, ch. 5, pp. 221–255.

[19] M. Ingels, G. Van der Plas, J. Crols, and M. Steyaert, "A CMOS 18 THzW 240 Mb/s transimpedance amplifier and 155 Mb/s LED-driver for low cost optical fiber links," *IEEE J. Solid-State Circuits*, vol. 29, pp. 1552–1559, Dec. 1994.

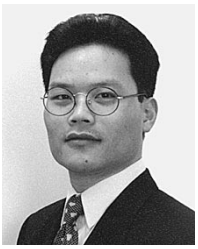

Khoman Phang received the B.A.Sc. and M.A.Sc. degrees in 1990 and 1992, respectively, from the University of Toronto, Toronto, ON, Canada, where he is currently working toward the Ph.D. degree in electronics.

In 1993, he was a Visiting Researcher at Sony Headquarters, Tokyo, Japan. He joined the Microelectronics Division of IBM, Toronto, Canada, in 1994, where he was involved in the development of infrared wireless networking products. He is presently a Lecturer in Electronics at the University of Toronto. His current research interests include optical receivers, infrared wireless data communications, and low-voltage analog integrated circuits.

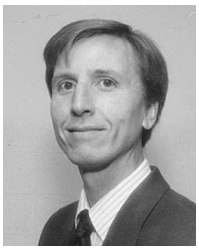

David A. Johns (S'81–M'89–SM'94) received the B.A.Sc., M.A.Sc. and Ph.D. degrees from the University of Toronto, Toronto, ON, Canada, in 1980, 1983, and 1989, respectively.

From 1980 to 1981, he was with Mitel and from 1983 to 1985, he was with Pacific Microcircuits Ltd. In 1988, he joined the University of Toronto, where he is currently a Full Professor. He has ongoing research programs in the general area of analog integrated circuits, with particular emphasis on circuits and systems for digital communications. His research has resulted in more than 40 publications and one textbook *Analog Integrated Circuit Design* (New York: Wiley, 1997), co-authored by K. Martin. He has been involved in numerous industrial short courses.

Dr. Johns served as an Associate Editor for IEEE TRANSACTIONS ON CIRCUITS AND SYSTEMS II from 1993 to 1995 and for IEEE TRANSACTIONS ON CIRCUITS AND SYSTEMS I from 1995 to 1997. He was a co-recipient of the 1999 IEEE Darlington Award.